Stopped-Flow Kinetic Investigations of the Activation of Soybean Lipoxygenase-1 and the Influence of Inhibitors on the Allosteric Site†

Viola C. Ruddat, Stephanie Whitman, Theodore R. Holman,* and Claude F. Bernasconi*

Department of Chemistry and Biochemistry, University of California, Santa Cruz, California 95064

Received December 11, 2002; Revised Manuscript Received February 3, 2003

ABSTRACT: Herein, we report on the role of the allosteric site in the activation mechanism of soybean lipoxygenase-1 utilizing stopped-flow inhibition kinetic studies. The K_D for the activation was determined to be 25.9 ± 2.3 μM and the rate constant for the oxidation of the iron cofactor, k_2, to be 182 ± 4 s^{-1}. Two inhibitors were employed in this study, (*Z*)-9-octadecenyl sulfate (OS) and (*Z*)-9-palmitoleyl sulfate (PS), of which OS is an allosteric inhibitor of the turnover process, while PS is a linear mixed inhibitor with a K_i of 13.7 ± 1.3 μM for the catalytic site and a K_i' of 140 ± 9 μM for the allosteric site. It was found that OS does not inhibit the activation of soybean lipoxygenase-1, while PS acts as a competitive inhibitor versus the product, 13-hydroperoxy-9,11-(*Z*,*E*)-octadecadienoic acid, with a K_i of 17.5 ± 3.8 μM. These results suggest that OS binds to an allosteric site that is separate from the catalytic iron site. We further observed that the allosteric site binding selectivity is sensitive to inhibitor length as seen by its preference for OS over that of PS, which is two carbons longer than PS.

Lipoxygenases are non-heme iron metalloproteins that are found in a wide variety of plants and animals. In plants, the lipoxygenase products are implicated in both senescence and germination (*1*, *2*). There are three major human lipoxygenases (HLO),[1] 5-, 12-, and 15-HLO, whose primary enzymatic difference is their positional specificity of action on arachidonic acid (AA) (*3*). These lipoxygenase products are the precursors to leukotrienes and lipoxins, which have been implicated as critical signaling molecules in a variety of diseases (*4*−*7*) such as asthma (*8*), prostate cancer (*9*), immune disorders (*10*), breast cancer (*11*, *12*), atherosclerosis (*13*), and colorectal cancer (*14*). These broad biological implications have elicited great interest in lipoxygenase as a potential therapeutic target and underscore the need for further studies of the lipoxygenase mechanism and inhibition.

Lipoxygenases regio- and stereospecifically oxygenate lipids, such as linoleic acid (LA) and AA, to form hydroperoxides (Scheme 1, Chart 1) (*15*, *16*). The inactive, ferrous enzyme is activated by the product, 13-hydroperoxy-9,11-(*Z*,*E*)-octadecadienoic acid (HPOD), through an inner sphere

Scheme 1: Activation of SLO by HPOD, Followed by the Catalytic Cycle

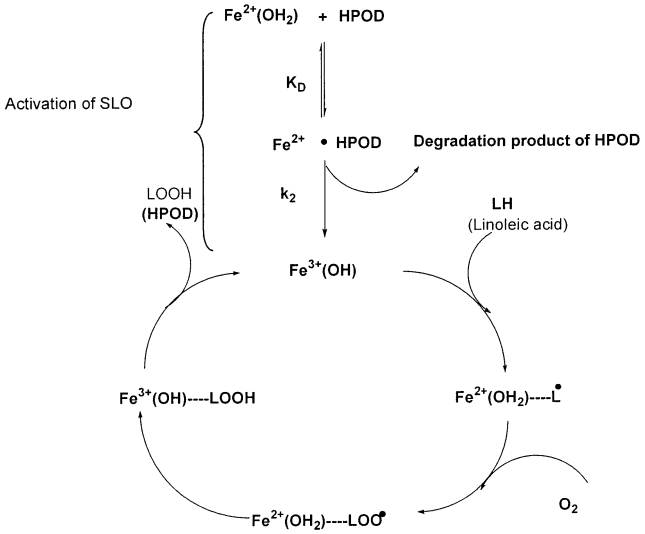

Chart 1: Structures of LA, HPOD, OS, and PS

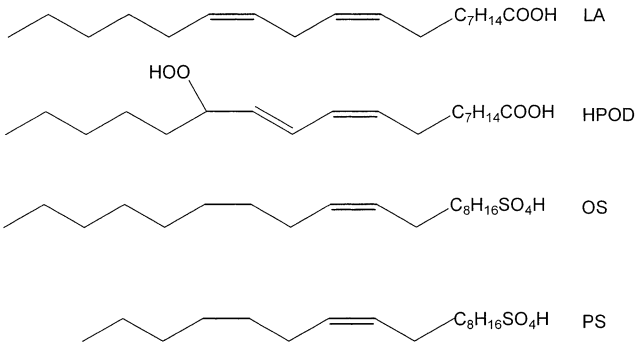

† This research has been supported by NIH Grant GM56062-01 and ACS Grant RPG-00-219-01-CDD (T.R.H.). Partial support of Viola Ruddat by the Department of Education in the form of a GANN fellowship is also gratefully acknowledged.

* To whom the correspondence should be addressed. E-mail: tholman@chemistry.ucsc.edu and bernasconi@chemistry.ucsc.edu.

[1] Abbreviations: HLO, human lipoxygenase; SLO, soybean lipoxygenase-1; HPOD, 13-hydroperoxy-9,11-(*Z*,*E*)-octadecadienoic acid; AA, archidonic acid; OPP, 4-(2-oxapentadeca-4-yne)phenyl propanoic acid; AKBA, acetyl-11-keto-β-boswellic acid; fatty sulfate, fatty acid with a sulfate group in place of a carboxyl group; OS, (*Z*)-9-octadecenyl sulfate; PS, (*Z*)-9-palmitoleyl sulfate; LS, linoleyl sulfate; AS, arachidonyl sulfate; K_i, dissociation constant of the inhibitor from the active site of the enzyme; K_i', dissociation constant of the inhibitor from the allosteric site of the enzyme; K_D, dissociation constant of the enzyme/HPOD complex; k_2, rate constant for the oxidation of the iron cofactor; k_{obsd}, the observed pseudo-first-order rate constant; HRESI-TOFMS, high-resolution, electron-spray-ionization, time-of-flight mass spectrometer; NMR, nuclear magnetic resonance; CMC, critical micelle concentration.

10.1021/bi020698o CCC: $25.00 © 2003 American Chemical Society
Published on Web 03/22/2003

oxidation to generate the active, ferric enzyme (*15*, *17*−*19*). If no HPOD is added, the enzyme displays a lag phase, which is due to the conversion of the ferrous enzyme to its ferric form by the product of the catalytic turnover, HPOD (*15*, *20*, *21*). The active site $Fe^{3+}(OH)$ then abstracts a hydrogen atom from the 1,4-diene moiety of the substrate, generating an $Fe^{2+}(OH_2)$ and a pentadienyl radical (*22*, *23*). The resulting radical is subsequently trapped by molecular oxygen and reduced to the hydroperoxide, re-establishing the $Fe^{3+}(OH)$ for the next catalytic cycle. Veldink and co-workers demonstrated that the enzyme could misfire and lose the pentadienyl radical intermediate, thus regenerating the inactive ferrous form (*24*, *25*). This is significant because it explains the unusual behavior in which the lag phase is dependent on both product and substrate concentrations.

Over the years, numerous inhibitors of lipoxygenase have been discovered with varying potency and selectivity (*5*−*7*). These inhibitors can be classified into two categories, redox and nonredox active. The redox active inhibitors are typically very potent but of little pharmaceutical value because of their tendency to produce toxic side effects (*26*−*30*). The nonredox active inhibitors are more relevant as therapeutic drugs, but their mode of action can be difficult to determine because of the multiple oxidation states of the enzymatic cycle. Marnett and Moody recently demonstrated that 4-(2-oxapentadeca-4-yne)phenylpropanoic acid (OPP), a selective inhibitor to leukocyte 12-HLO, binds to the active site of both the ferric and the ferrous forms of lipoxygenase (*31*). In fact, OPP binds to the ferrous form over ≈ 300-fold more tightly than to the ferric form. This discovery indicates that one can design inhibitors that preferentially bind to the inactive ferrous form of lipoxygenase, thus never allowing the enzyme to become active; a very potent mode of inhibition.

The design and mechanistic characterization of specific inhibitors becomes more complicated when one considers the possibility of an allosteric site that is separate from the active site. Aharony and Stein were the first to suggest the possible existence of a regulatory site (*32*). They found that at high substrate concentrations, two independent sites are occupied. Furthermore, Safayhi et al. showed that acetyl-11-keto-β-boswellic acid (AKBA) covalently modified 5-HLO while the enzyme retained some catalytic activity, suggesting the presence of an allosteric site (*33*). The hypothesis was further substantiated when our lab discovered that (*Z*)-9-octadecenyl sulfate (OS) (Chart 1) manifested hyperbolic dependence on inhibitor concentration in steady-state inhibition kinetics for SLO, with an allosteric site K_I' of 0.6 μM and a catalytic site K_i of >18 μM (*34*). It should be noted that the natural substrate for SLO, LA, also binds to the allosteric site but with a much lower binding constant than OS (K_i > 30 μM) (*34*). More recently, Marnett and Moody observed mixed inhibition of OPP with the ferric form of 12-HLO, with OPP binding to both the catalytic and the allosteric sites (K_i = 2 μM and K_i' = 4.5 μM, respectively) (*31*). This leads us to the question of what role does the allosteric site play in the activation/catalytic mechanism of SLO, and what are the structural selectivity differences between the allosteric site and the catalytic sites?

In the current study, we have investigated the presence of the allosteric site in SLO further by monitoring the rate of activation (i.e., iron oxidation) through stopped-flow kinetics. We have synthesized a novel inhibitor, (*Z*)-9-palmitoleyl sulfate (PS) (Chart 1), which binds to the catalytic site and, using stopped flow kinetics, have investigated whether PS and OS compete with HPOD for the iron catalytic site. The results presented here have broad implications regarding inhibition of lipoxygenase because the allosteric and catalytic sites may have different structure/activity relationships and thus may have different pharmacokinetic profiles.

MATERIALS AND METHODS

Materials. SLO was expressed and purified as described previously (*35*). Iron content of SLO was determined on a Finnegan inductively coupled plasma mass spectrometer (ICP-MS), using an internal Co^{3+} standard and external standardized iron solution. We standardized all enzyme concentrations to iron content since only ≈ 80% of the enzyme contains the iron cofactor and only enzyme with the iron is active.

Fatty Sulfate Synthesis. PS ($C_{16}H_{32}O_4S$) was prepared by a similar procedure to that of Axelrod and co-workers (*36*) and as previously described for OS (*34*). One gram of the fatty alcohol (Nu-Chek-Prep, Inc.) was dissolved under nitrogen in 6 mL of dry pyridine, and 0.5 g of sulfamic acid were added. The reaction mixture was heated at 95 °C for 1.5 h under nitrogen and quenched with the addition of 20 mL of methanol and 1 mL of saturated Na_2CO_3. The waste solids were removed by filtration, and the solution was evaporated to dryness. The resulting residue was recrystallized from hot methanol, and the white solid gave a single spot by TLC (silica gel), developed in hexane/ether/acetic acid (60:39:1). The ^1H NMR signals ($CDCl_3$) for PS were observed at δ 5.35 (br m, 2H), 4.02 (t, 2H), 2.01 (br m, 4H), 1.65 (br m, 2H), 1.30 (br m, 18H), 0.89 (t, 3H). OS was obtained as previously described (*34*).

Fatty Acid Purification. LA was purchased from Aldrich Chemical Co., and HPOD was produced by reaction of LA with SLO, exhaustively extracted with CH_2Cl_2 and purified by a Waters 625 HPLC with a C18 column (Higgins Analytical, 5 micron, 250 × 10 mm, isocratic mobile phase: 86.9% methanol:13% H_2O:0.1% acetic acid at 3 mL/min). HPOD was detected by on-line UV absorption (210 nm) and had a retention time of approximately 30 min. Product fractions were collected, evaporated to dryness, redissolved in ethanol, and stored at −20 °C.

Fatty Sulfate Quantitation. PS and OS were dissolved in water, and their concentration was determined by NMR using an internal standard of linoleyl sulfate (LS) as described previously (*34*). LS concentrations were determined by using SLO to convert 100% of the LS to the hydroperoxide product (ϵ = 25 000 M^{-1} cm^{-1}, assuming a similar ϵ to that of HPOD). Aqueous fatty sulfate solutions containing fixed amounts of LS were analyzed by NMR ($CDCl_3$), and their relative ratios were determined by comparing their signal integrations.

Surface Tension Measurements. Borate buffers were used, which correspond to those of the kinetic measurements. Surface tension was measured as described previously by our group, using a thin platinum plate (perimeter 2.5 cm) and a Cahn electro-microbalance (*37*). Various amounts of fatty sulfates were added to a 30 mL buffer solution, and the surface tension was continuously recorded. After each

addition, a sufficiently long period of time (≈ 10−30 min) was allowed to elapse before attaining a steady value of the surface tension. Critical micelle concentration (CMC) values were obtained by plotting the measured surface tensions versus the logarithm of the concentrations of the surface-active agent and recording the intercept of the two straight lines. The point of deviation from the straight line, as observed in the surface tension versus log [surface-active agent] plot, was defined as the start of pre-micellular aggregate formation (an example of this plot can be found in the Supporting Information) (*37*, *38*).

Destruction of HPOD by SLO. Determination of the destruction of HPOD by ferrous SLO was similar to that previously published by Holman and co-workers for the kinetic isotope effect, with the following modifications (*39*). Either HPOD was titrated into SLO or SLO was titrated into HPOD up to a final concentration of 2.2 μM in 4 mL for the second added reactant. The solution was acidified with 400 μL of acetic acid and then extracted with methylene chloride. The methylene chloride layer was evaporated to dryness under vacuum, reconstituted in 50 μL of running buffer, injected onto a C18 column (Higgins Analytical, 5 micron, 250 × 4.6 mm), and eluted at 1 mL/min (isocratic mobile phase: 74.9% methanol:25% H_2O:0.1% acetic acid). The elution peaks were then compared to a separate injection of a known amount of HPOD and quantified. This extraction procedure retrieved over 90% of the sample when no SLO was added.

Isolation of the Unknown Peak. The unknown compound that was generated upon addition of SLO to HPOD was isolated by a series of 20 injections of the above reaction mixture, and the corresponding peaks were collected. The collected samples were evaporated, and the exact mass was determined on a high-resolution, electron-spray-ionization, time-of-flight mass spectrometer (HRESI-TOFMS).

Steady-State Kinetics and Inhibition Studies. The turnover rates of SLO were determined by following the formation of HPOD at 234 nm (ϵ = 25 000 M^{-1} cm^{-1}) with a Hewlett-Packard 8453 UV−vis spectrophotometer. The photochemical destruction of HPOD by the UV light of the diode array spectrophotometer was negligible under these reaction conditions. All reaction solutions contained 2 mL of 0.1 M borate (pH 9.2), and the reactions were run at room temperature (23 °C) under constant stirring with a rotating magnetic bar. Substrate solutions used in each experiment were measured for accurate LA concentration by quantitatively converting substrate to product using SLO. Enzymatic rates were measured at concentrations between 1 and 50 μM LA with 1−40 μM PS for SLO. Solutions containing LA and/or PS were sonicated for 3−5 min before use in kinetic experiments. Kinetic runs were initiated by the addition of enzyme to final concentrations of ≈ 3 nM SLO (≈ 80% iron content), and all kinetic parameters were determined by nonlinear regression using Kaleidagraph software (Synergy Software) (an example of these plots can be found in the Supporting Information). Each rate constant is the average of three determinations.

Stopped-Flow Kinetics. Sodium borate buffer, 0.1 M, at pH 9.2 was used for all experiments. The kinetic measurements of the activation were carried out under pseudo-first-order conditions with the enzyme as the minor component. Both the HPOD and the inhibitor were added at 10-fold or greater concentration in excess of the amount of SLO. The solutions of enzyme, HPOD, and inhibitors were prepared immediately before the kinetic experiments. The concentrations of enzyme and HPOD were verified in an Agilent 8453 UV−vis spectrophotometer at λ_{max} = 234 nm for the HPOD and λ_{max} = 280 nm for the enzyme. The extinction coefficient for SLO was 1.34 × 10^5 M^{-1} cm^{-1}. The stopped-flow studies were carried out on a DX.17MV Applied Photophysics spectrofluorometer equipped with a 150-W xenon arc lamp light source. The changes in fluorescence above 320 nm were monitored using a 320 nm cutoff filter in front of the photomultiplier (exciting wavelength 280 nm). All kinetic parameters were determined using the nonlinear regression software by Jandel Scientific. All experiments were carried out at 25 °C. To determine K_D and k_2, kinetic runs were performed at 13 different HPOD concentrations; each pseudo-first-order rate constant (k_{obsd}) is the average of at least five determinations. The stopped-flow apparatus was rinsed with HNO_3, KOH, and water after every couple of runs to prevent enzyme buildup and thus artifacts in the kinetics.

Stopped-Flow Inhibition Studies. The inhibitor was allowed to equilibrate with the enzyme for 15 min but was used within 30 min of preparation. The determination of K_i was carried out at eight different inhibitor concentrations, each at 4-, 10-, and 20-fold excess HPOD over enzyme.

RESULTS

Protein Purification. SLO was purified with yields of ≈4 mg/L and metal content of 80 ± 5% (*35*).

Surface Tension Measurements. The CMC of PS and OS in 100 mM borate (pH 9.2) were determined as previously reported (*34*). OS had a CMC of 18 ± 6 μM, and PS had a CMC of 70 ± 15 μM, which are consistent with the CMC values of similar fatty sulfates (*34*).

Comparison of k_{obsd} as Determined by Fluorescence and Absorbance. The rates of iron oxidation can be determined in the absorbance mode (330 nm) as well as in the fluorescence mode (350 nm). The kinetics were carried out at high enzyme concentrations to ensure reasonable amplitude. The k_{obsd} values (k_{obsd} refers to the observed pseudo-first-order rate constant) from the absorbance measurements were the same as those determined by fluorescence.

Kinetic Determination of K_D and k_2. The activation of SLO can be described by

$$Fe^{2+}(OH_2) + HPOD \underset{k_{-1}}{\overset{k_1}{\rightleftharpoons}} Fe^{2+}\bullet HPOD \xrightarrow{k_2} Fe^{3+}(OH) + \text{unknown} \quad (1)$$

In the analysis to follow, we will use the following definitions: $(k_{-1} + k_2)/k_1 = K_m$ and since $k_{-1} \gg k_2$, $K_m = K_D$ (*38*, *40*). We will use K_D from hereon. Rates of the formation of Fe^{3+}(OH) were measured by monitoring the change in fluorescence of the enzyme above 320 nm (*38*, *40*). Pseudo-first-order rate constants were determined between 1.5 and 200 μM HPOD. Figure 1 shows a plot of k_{obsd} versus [HPOD]; it represents a saturation curve consistent with an accumulation of Fe^{3+}•HPOD at high concentrations. The expression for k_{obsd} is given in eq 2.

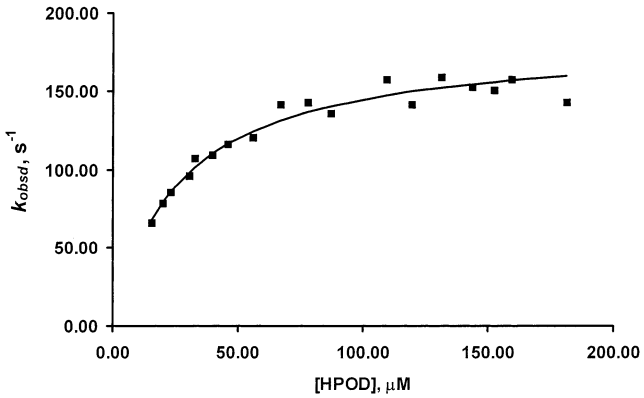

FIGURE 1: Plot of k_{obsd} for the activation of SLO vs HPOD concentration; experimental points (■) and theoretical fit (−). The reaction was monitored by flourescence in the stopped-flow apparatus, $[Fe^{2+}(OH_2)] = 3.03$ μM. All data points shown represent averages of five measurements.

$$k_{obsd} = \frac{k_2[HPOD]}{K_D + [HPOD]} \quad (2)$$

Using nonlinear regression methods, the dissociation constant, K_D, was determined to be 25.9 ± 2.3 μM. The rate constant for the rate determining second step, k_2, was found to be 182 ± 4 s^{-1}.

Inhibition Studies. Scheme 2 shows the kinetic scheme in the presence of a competitive inhibitor. The expression for k_{obsd} based in Scheme 2 with both HPOD and PS in excess at all times is shown in eq 3.

Scheme 2: Activation of SLO by HPOD, Including the Inhibition by PS

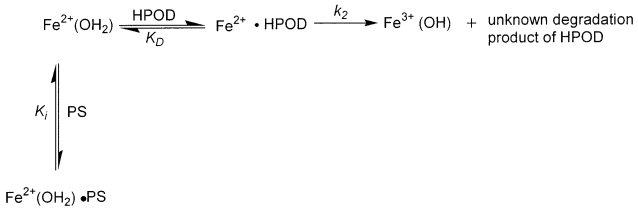

$$k_{obsd} = k_2 \frac{(1/K_D)[HPOD]}{(1 + (1/K_D)[HPOD] + (1/K_i)[PS])} \quad (3)$$

The dependence of k_{obsd} on inhibitor concentration was determined at 13 different inhibitor concentrations up to 30 μM; we did not raise the inhibitor concentration further because the CMC values for both PS and OS indicated that higher inhibitor concentrations would not increase the free inhibitor concentration. Indeed, we found that at higher PS concentrations, the k_{obsd} began to level off, indicating saturation of the free PS concentration.

Each kinetic run was repeated at least five times. The data were analyzed based on the inverse plot according to eq 4. A typical plot is shown in Figure 2.

$$\frac{1}{k_{obsd}} = \frac{1/K_i}{k_2(1/K_D)[HPOD]}[PS] + \frac{1}{k_2} + \frac{1}{k_2(1/K_D)[HPOD]} \quad (4)$$

From a plot of the $1/k_{obsd}$ versus the inhibitor concentration, K_i for PS was determined from the slope to be 17.5 ± 3.8 μM. By plotting the y intercept of eq 4 versus 1/[HPOD], and using k_2 determined previously, K_D can be calculated from the slope to be 25.4 ± 2.0 μM, in excellent agreement with K_D calculated from the saturation curve in the absence of inhibitor. All kinetic data is summarized in Table 1.

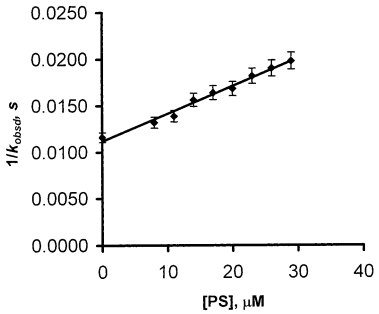

FIGURE 2: Plot of $1/k_{obsd}$ vs [PS] concentration according to eq 4 for the determination of K_i. The reactions were monitored by fluorescence in the stopped-flow apparatus, [HPOD] = 22.5 μM, $[Fe^{2+}(OH_2)] = 2.0$ μM. All data points shown represent averages of five measurements.

Table 1: Kinetic Parameters of the Activation of SLO and Its Inhibition

K_D[a] (μM)	K_D[b] (mM)	k_{cat} (s^{-1})	K_i (PS)[c] (μM)	K_i (PS)[d] (μM)	K_i' (PS)[e] (μM)
25.9 ± 2.3	25.4 ± 2.0	182 ± 4	17.5 ± 3.8	13.7 ± 1.3	140 ± 9

[a] K_D determined from stopped-flow saturation data of the activation. [b] K_D determined from stopped-flow inhibition data of the activation. [c] K_i of the active site determined from stopped-flow inhibition data. [d] K_i of the active site determined from steady-state data for the turnover. [e] K_i' of the allosteric site determined from the steady-state data for the turnover.

Scheme 3: Linear Mixed Inhibition of SLO (E) by PS in Presence of Substrate (LA)

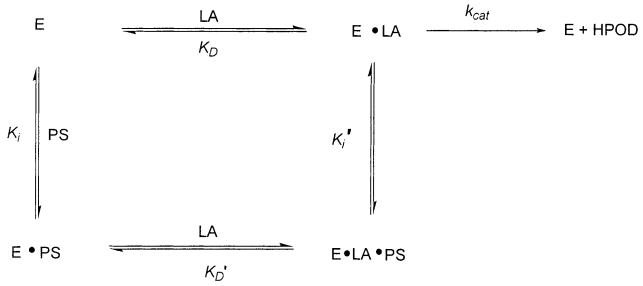

Steady-State Inhibition Kinetics of SLO and PS. The steady-state kinetic parameters of the catalytic turnover of LA to HPOD were determined for SLO in the presence of PS. The possible mode of inhibition is shown in Scheme 3. For each experiment, the enzyme and inhibitor concentration was held constant. The rate, v, of the reaction was measured in terms of the appearance of HPOD as a function of [SLO], [LA], and [PS] (eq 5).

$$v = \frac{k_{cat}[E]_0[LA]}{K_m + [LA] + \frac{K_m[PS]}{K_i} + \frac{[LA][PS]}{K_i'}} \quad (5)$$

K_i is defined as the equilibrium constant of the dissociation of the inhibitor PS from the catalytic site, K_i' is the equilibrium constant of the dissociation of the inhibitor PS from the allosteric site, v is the observed steady-state rate,

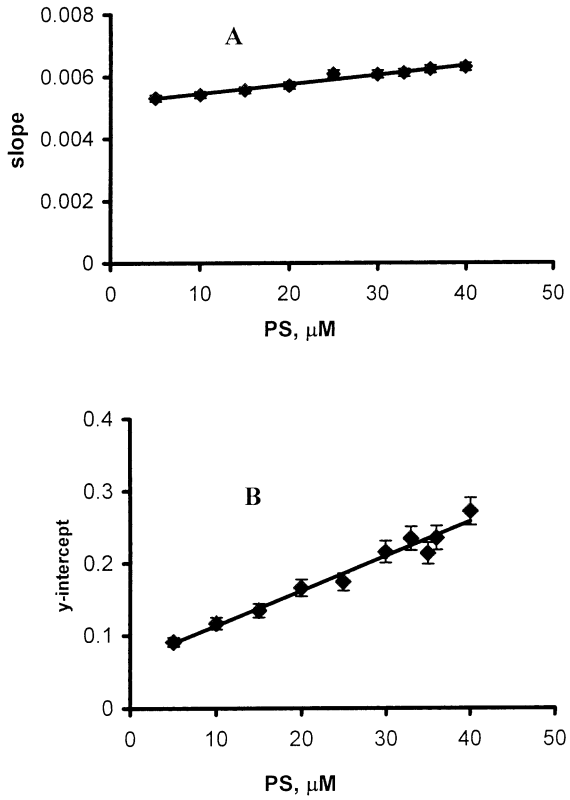

FIGURE 3: Steady-state data for the determination of K_i and K_i' for SLO with PS. Figure 4A represents the secondary re-plot of the inhibition data as the *y* intercepts vs [PS], while Figure 4B represents the secondary re-plot of the inhibition data as the slope vs [PS]. All data points shown represent averages of three measurements.

and k_{cat} and K_m are the values from the Michaelis−Menten fits. Rearranging eq 5 yields eq 6.

$$\frac{[E]_0}{v} = \frac{K_m}{k_{cat}}\left(1 + \frac{[PS]}{K_i}\right)\frac{1}{[LA]} + \frac{1}{k_{cat}}\left(1 + \frac{[PS]}{K_i'}\right) \quad (6)$$

Plotting $[E]_0/v$ versus 1/[LA], at constant [PS] according to eq 6 (plots not shown), affords a slope given by eq 7 and a *y* intercept given by eq 8.

$$\text{slope} = \frac{K_m}{k_{cat}}\left(1 + \frac{[PS]}{K_i}\right) \quad (7)$$

$$y\ \text{intercept} = \frac{1}{k_{cat}}\left(1 + \frac{[PS]}{K_i'}\right) \quad (8)$$

This experiment was carried out at a number of different inhibitor concentrations. The plots of slopes and *y* intercepts versus [PS] are shown in Figure 3A and 3B, respectively. These plots, in turn, provide slopes and *y* intercepts as follows: $K_m/(K_i k_{cat})$ (slope for Figure 3A), K_m/K_i (*y* intercept for Figure 3A); $1/(k_{cat}K_i')$ (slope for Figure 3B), and $1/k_{cat}$ (*y* intercept for Figure 3B). If only one mode of inhibition was taking place, the K_i determined from either plot would be the same. This is not the case here, indicating that SLO exhibits a linear mixed inhibitor response. Fitting the data to this model yielded a K_i of 13.7 ± 1.3 μM for the active site and a K_i' of 140 ± 9 μM for the allosteric site, a more than 10-fold difference (*31*, *41*−*43*).

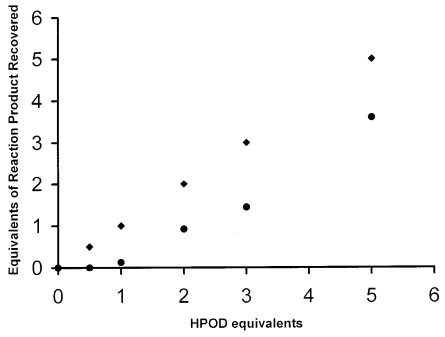

FIGURE 4: Reaction of SLO with HPOD: plot of recovered HPOD (●) and theoretical recovery of 100% HPOD (♦) vs equivalents of HPOD added.

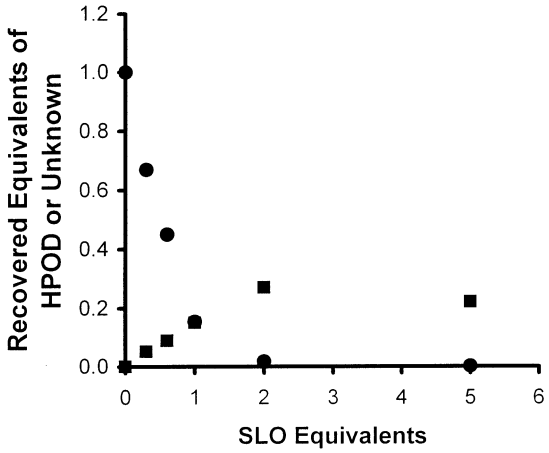

FIGURE 5: Reaction of SLO with HPOD: plot of recovered HPOD (●) and unknown compound (■) vs equivalents of SLO. The unknown has a λ_{max} of 234 nm, similar to HPOD, and is assumed to have the same extinction coefficient.

Destruction of HPOD by SLO. HPOD was titrated into 4 mL of 4.4 μM SLO until 5 equiv had been added; the products were then extracted and analyzed by HPLC. The amount of recovered HPOD was minimal up until approximately 1 equiv of HPOD had been added, at which point HPOD started to appear on the HPLC (Figure 4). SLO was then titrated into 4 mL of 4.4 μM HPOD and analyzed in the same way as above. The amount of HPOD decreased linearly with the addition of SLO until no HPOD was left at approximately 1 equiv of SLO (Figure 5). It should be noted that in both cases a slight excess of SLO was needed to consume the HPOD fully. This is explained by the fact that SLO only has 80 ± 5% of the iron that is required for HPOD destruction.

Isolation of the Unknown Peak. The destruction of HPOD by the addition of SLO results in a new compound at half the HPLC retention time of HPOD and appears inversely with that of HPOD loss. The new peak has an absorption maximum at 234 nm, identical to that of HPOD. Considering that this unknown compound has the same absorption spectrum as HPOD, we can assume that the conjugated diene remains intact and that its extinction coefficient is the same as HPOD. If this is assumed, only 25% of total HPOD concentration is converted to the unknown compound, suggesting this peak is a minor product in the destruction of HPOD. The remaining 75% of HPOD are not visible under the current conditions. The consumption of over 40 mg of SLO produced enough of the unknown compound to measure

its mass by HRESI-TOFMS to be 309.0260 g/mol. This exact mass matches with a molecular formula of $C_{18}H_{29}O_4$ (MW calcd = 309.2066 g/mol) and corresponds to a loss of two hydrogen atoms from the product, HPOD.

DISCUSSION

For many years, inhibition studies have been performed on lipoxygenase, and key mechanistic aspects have been determined. In general, there are three broad categories that characterize the mode of inhibition: competitive, reductive, and allosteric (*6*, *44*). The competitive inhibitors bind to the catalytic site, while the reductive inhibitors convert the active ferric enzyme to the inactive ferrous form (*45*, *46*). The allosteric inhibitors, however, have markedly different kinetic properties, which do not fit standard inhibition models (*31*, *34*). One such example is OS, a novel inhibitor to lipoxygenase synthesized in our lab, which displayed kinetic properties that could not be fitted with a simple competitive kinetic model. The steady-state kinetic data could be matched with a hyperbolic mixed inhibition model. With this kinetic model, we determined that OS bound to the allosteric site ($K_i' = 0.6\ \mu$M) and caused an approximately 4-fold increase in the apparent K_m (*34*).

OS is very similar in size to LA, the natural substrate of SLO; however, it binds preferentially to the allosteric site, while LA binds preferentially to the catalytic site (*34*). These catalytic and allosteric site selectivity differences between OS and LA may be due to the fact that OS is two atoms longer and more polar because of the sulfate group. To test this hypothesis, we synthesized a new inhibitor, PS, which has the same length as LA but has the polar sulfate group of OS. We reasoned that the size similarity to LA would instill a binding selectivity for PS to the active site over that of the allosteric site, opposite to the selectivity of OS. This turned out to be correct, with the binding potency of PS to the catalytic site increasing ($K_i = 13.7\ \mu$M) and the binding potency to the allosteric site decreasing ($K_i' = 140\ \mu$M), relative to OS ($K_i \gg 18\ \mu$M and $K_i' = 0.6\ \mu$M, respectively). This indicates that the allosteric site has a binding preference for larger, mono-unsaturated, sulfates. It is interesting to note that the catalytic site is less sensitive to length then the allosteric site, as seen by the similar K_m values of $\approx 12\ \mu$M for LA, linoleyl sulfate (LS), AA, and arachidonyl sulfate (AS), all of which have varying lengths (the K_m values are an upper limit to the true K_D) (*36*, *47*). The key difference between these substrates and the fatty sulfate inhibitors is the degree of conjugation, which will add additional rigidity to the substrates. The difference in rigidity possibly explains the preference of these compounds for the catalytic site over the allosteric site and may indicate a structural difference between the two sites. We are currently investigating the location of the allosteric site and possible amino acid interactions, with the objective of defining the allosteric site further.

The results described above address the question of how the allosteric site affects the steady-state catalytic turnover, but they do not address how the allosteric site affects activation (i.e., the conversion of the ferrous state to the ferric state). Stopped-flow kinetics have been previously used to investigate the mechanism of activation. Jones et al. monitored the decrease in the tryptophan fluorescence because of the oxidation of the iron and determined that the second-order rate constant of activation is $\approx 6.7 \times 10^6\ M^{-1}\ s^{-1}$ (*48*). In the current paper, we have also monitored this process with stopped-flow fluorescence and confirm their results. More importantly, we were able to extend the concentration range and achieve saturation of the activation rate (Figure 1). This allowed us to calculate the K_D, k_2, and k_2/K_D for activation to be $25.9 \pm 1.5\ \mu$M, $182 \pm 4\ s^{-1}$, and $6.8 \times 10^6 \pm 0.54\ M^{-1}\ s^{-1}$, respectively. These values correlate well with previous results by Schilstra et al., who used numerical integration methods, assuming a single binding site, to approximate the dissociation constant of the HPOD/enzyme complex to be 24 μM (*19*). Similarly, our data agrees with Verhagen's, who estimated an approximate k_2 for oxidation to be $150\ s^{-1}$ from initial rate measurements (*38*). We also monitored the increase in absorbance at 330 nm, which corresponds to the ferric ligand-to-metal charge-transfer band and determined that the increase at 330 nm had the same rate as the Trp fluorescence decrease. These results support the previous observations of an increase in absorbance at 330 nm upon HPOD addition and a corresponding decrease in Trp fluorescence because of Forester energy transfer with the ferric ion (*17*, *21*, *25*, *49*, *50*). This correlation between the absorbance and the fluorescence data was also verified by EPR studies that confirmed the existence of the high spin ferric species (*16*).

The activation of SLO is the result of the direct interaction between HPOD and iron, which leads to an inner sphere electron transfer, as has been demonstrated by structural and kinetic studies (*17*, *19*, *20*, *25*, *38*). However, it should be noted that this inner sphere oxidation hypothesis was questioned by a single publication, which reported no destruction of HPOD upon addition to the ferrous SLO (*48*). This latter claim is at odds with our results, which clearly demonstrate a one-to-one destruction of HPOD by ferrous SLO. In addition, we detected a corresponding increase of an unknown compound (MW = 309.0260 g/mol) at 25% recovery, whose exact mass matches $C_{18}H_{29}O_4$. This unknown compound is most likely the result of a radical side reaction from the HPOD degradation product and will require further study with a large quantity of enzyme to identify its exact structure by NMR. The bulk of the reacted HPOD (75%) is not recovered because of its ability to dimerize and react with protein side chains and/or the buffer, as previously observed (*51*). Our results are all in accordance with the majority of the previously published data that indicates an inner sphere oxidation mechanism, in which the HPOD binds directly to the iron.

The activation process is an ideal tool for monitoring the mode of inhibition by a particular molecule because a competitive inhibitor should block the inner sphere oxidation and hence activation. An allosteric inhibitor would not compete with HPOD for the iron active site because it binds to a separate site. As stated previously, PS is an inhibitor of the catalytic site, with a steady-state K_i of $13.7 \pm 1.3\ \mu$M. Upon addition of PS to the reaction solution in the stopped-flow experiment, inhibition of the activation was observed with a K_i of $17.5 \pm 3.8\ \mu$M. This K_i value is indistinguishable from that obtained from the steady-state kinetics (within experimental error limits) and confirms that PS binds to the active site, inhibiting the inner sphere oxidation of the iron by HPOD. Addition of OS to the stopped-flow experiment,

however, had no effect on activation up to its CMC concentration of 18 μM. This is in complete agreement with the previous steady-state allosteric inhibition results (*34*) and indicates that OS binds selectively to the allosteric site and not appreciably to the catalytic site. This result also indicates that OS binding to the allosteric site has no affect on the activation rate; thus, its role is solely in affecting the catalytic rate of the ferric catalytic process.

The presence of an allosteric site is significant with regards to the design of lipoxygenase inhibitors since it opens the possibility of a new class of inhibitors. One could postulate that the three classes of nonredox inhibitors, allosteric, ferrous catalytic, and ferric catalytic, could have distinct pharmacological effects and thus different therapeutic roles.

ACKNOWLEDGMENT

Professor Crews is gratefully acknowledged for the use of his HRESI-TOFMS.

SUPPORTING INFORMATION AVAILABLE

Three plots. This material is available free of charge via the Internet at http://pubs.acs.org.

REFERENCES

1. Gardner, H. W. (1991) *Biochim. Biophys. Acta 1084*, 221−239.
2. Siedow, J. N. (1991) *Annu. Rev. Plant Physiol. Plant Mol. Biol. 42*, 145−188.
3. Brash, A. R. (1999) *J. Biol. Chem. 274*, 23679−23682.
4. Sigal, E. (1991) *J. Am. Phys. Soc. 260*, 13−28.
5. Samuelsson, B., Dahlen, S. E., Lindgren, J. A., Rouzer, C. A., and Serhan, C. N. (1987) *Science 237*, 1171−1176.
6. Steele, V. E., Holmes, C. A., Hawk, E. T., Kopelovich, L., Lubet, R. A., Crowell, J. A., Sigman, C. C., and Kelloff, G. J. (1999) *Cancer Epidemmiol. Biomarkers Prev. 8*, 467−483.
7. Dailey, L. A., and Imming, P. (1999) *Curr. Med. Chem. 6*, 389−398.
8. Nakano, H., Inoue, T., Kawasaki, N., Miyataka, H., Matsumoto, H., Taguchi, T., Inagaki, N., Nagai, H., and Satoh, T. (2000) *Bioorg. Med. Chem. 8*, 373−380.
9. Gosh, J., and Myers, C. E. (1998) *Proc. Natl. Acad. Sci. 95*, 13182−13187.
10. Hussain, H., Shornick, L. P., Shannon, V. R., Wilson, J. D., Funk, C. D., Pentland, A. P., and Holtzman, M. J. (1994) *Am. J. Physiol. 266*, C243−C253.
11. Connolly, J. M., and Rose, D. P. (1998) *Cancer Lett. 132*, 107−112.
12. Natarajan, R., and Nadler, J. (1998) *Front. Biosci. 3*, E81−88.
13. Harats, D., Shaish, A., George, J., Mulkins, M., Kurihara, H., Levkovitz, H., and Sigal, E. (2000) *Arterioscler. Thromb. Vasc. Biol. 20*, 2100−2105.
14. Kamitani, H., Geller, M., and Eling, T. (1998) *J. Biol. Chem. 273*, 21569−21577.
15. Schilstra, M. J., Veldink, G. A., and Vliegenhart, J. F. G. (1993) *Biochemistry 32*, 7686−7691.
16. De Groot, J. J., Veldink, G. A., Vliegenhart, J. F. G., Boldinngh, J., Wever, R., and van Gelder, B. F. (1975) *Biochim. Biophys. Acta 377*, 71−79.
17. Egmond, M. R., Fasella, P. M., Veldink, G. A., Vliegenthart, J. F., and Boldingh, J. (1977) *Eur. J. Biochem. 76*, 469−479.
18. Ludwig, P., Holzhutter, H. G., Colosimo, A., Silvestrini, M. C., Schewe, T., and Rapoport, S. M. (1987) *Eur. J. Biochem. 168*, 325−337.
19. Schilstra, M. J., Veldink, G. A., Verhagen, J., and Vliegenhart, J. F. G. (1992) *Biochemistry 31*, 7692−7699.
20. Skrzypczak-Jankun, E., Bross, R., Carroll, R., Dunham, W., and Funk, M. (2001) *J. Am. Chem. Soc. 123*, 10814−10820.
21. Egmond, M. E., Finnazzi-Agro, A., Fasella, P., Veldink, G., and Vliegenhart, J. F. G. (1975) *Biochim. Biophys. Acta 397*, 43−49.
22. Tomchick, D. R., Phan, P., Cymborowski, M., Minor, W., and Holman, T. R. (2001) *Biochemistry 40*, 7509−7517.
23. Scarrow, R. C., Trimitsis, M. G., Buck, C. P., Grove, G. N., Cowling, R. A., and Nelson, M. J. (1994) *Biochemistry 33*, 15023−15035.
24. Schilstra, M. J., Veldink, G. A., and Vliegenhart, J. F. G. (1994) *Lipids 29*, 225−231.
25. Schilstra, M. J., Veldink, G. A., and Vliegenhart, J. F. G. (1994) *Biochemistry 33*, 3974−3979.
26. Falhueyret, J. P., Hutchinson, J. H., and Riendeau, D. (1993) *Biochem. Pharmacol. 45*, 978−981.
27. Bird, T., Geoffrey, C., Bruneau, P., Crawley, G. C., Edwards, M. P., Foster, S. J., Girodeau, J. M., Kingston, J. F., and McMillan, R. M. (1991) *J. Med. Chem. 34*, 2176−2186.
28. Ducharme, Y., Brideau, C., Dube, D., Chan, C. C., Falgueyret, J. P., Gillard, J. W., Fuay, J., Hutchinson, J. H., McFarlane, C. S., Riendeau, D., Schneugetz, J., and Girard, Y. (1994) *J. Med. Chem. 37*.
29. Delorme, D., Ducharme, Y., Brideau, C., Chan. C. C., Chauret, N., Desmarais, S., Dube, D., Falgueyret, J. P., Fortin, R., Guay, J., Hamel, P., Jones, T. R., Lepine, C., Li, C., McAuliffe, M., McFarlane, C. S., Nicoll-Griffith, D. A., Riendeau, D., Yergey, J. A., and Girard, Y. (1996) *J. Med. Chem. 39*, 3951−3970.
30. Hamel, P., Riendeau, D., Brideau, C., Chan, C. C., Demarais, S., Delorme, D., Dube, D., Ducharme, Y., Ethier, D., Grimm, E., Falgueyret, J. P., Guay, J., Jones, T. R., Dwong, E., McAuliffe, M., McFarlane, C. S., Piechuta, H., Roumi, M., Tagari, P., Young, R. N., and Girard, Y. (1997) *J. Med. Chem. 40*, 2866−2875.
31. Moody, J. S., and Marnett, L. J. (2002) *Biochemistry 41*, 10297−10303.
32. Aharony, D., and Stein, R. (1986) *Eur. J. Biochem. 261*, 133−142.
33. Safayhi, H., Mack, T., Sabieraj, J., Anazodo, M., Subramanian, L., and Ammon, H. (1992) *J. Pharmacol. Exp. Therapeut. 261*, 1143−1146.
34. Mogul, R., Johansen, E., and Holman, T. R. (2000) *Biochemistry 39*, 4801−4807.
35. Holman, T. R., Zhou, J., and Solomon, E. I. (1998) *J. Am. Chem. Soc. 120*, 12564−12572.
36. Bild, G. S., Ramadoss, C. S., and Axelrod, B. (1977) *Lipids 12*, 732−735.
37. Harkins, W. D., and Anderson, T. F. (1937) *J. Am. Chem. Soc. 59*, 2189−2197.
38. Verhagen, J., Veldink, G. A., Egmond, M. R., Vliegenthart, J. F. G., Boldingh, J., and van der Star, J. (1978) *Biochim. Biophys. Acta 529*, 369−79.
39. Lewis, E. R., Johansen, E., and Holman, T. R. (1999) *J. Am. Chem. Soc. 121*, 1395−1396.
40. Egmond, M. E., Fasella, P. M., Veldink, G. A., Vliegenhart, J. F. G., and Boldingh, J. (1977) *Eur. J. Biochem. 76*, 469−479.
41. Segel, I. H. (1975) *Enzyme Kinetics*, John Wiley and Sons, Inc., New York.
42. Dixon, M. (1953) *Biochemistry 55*, 170−171.
43. Cornish-Bowden, A. (1974) *Biochemistry 137*, 143−144.
44. Steele, V., Holmes, C. A., Hawk, E. T., Kopelovich, R. A., Lubet, R. A., Crowell, J. A., Sigman, C. C., and Kelloff, G. J. (2000) *Exp. Opin. Invest. Drugs 9*, 2121.
45. Zherebtsov, N. A., Popova, T. N., and Zyablova, T. V. (2000) *Biochemistry 65*, 620.
46. Kemal, C., Louis-Flamberg, P., Krupinski-Olsen, R., and Shorter, A. (1987) *Biochemistry 26*, 7064−7072.
47. Mogul, M., and Holman, T. R. (2001) *Biochemistry 40*, 4391−4397.
48. Jones, G. D., Russell, L., Darley-Usmar, V. M., Stone, D., and Wilson, M. T. (1996) *Biochemistry 35*, 7197−7203.
49. Egmond, M. R., and Williams, R. J. (1978) *Biochim. Biophys. Acta 531*, 141−148.
50. Finazzi Agro, A., Avigliano, L., Egmond, M. R., Veldink, G. A., and Vliegenthart, F. G. (1975) *FEBS Lett. 52*, 73−76.
51. Chamultriat, W., and Mason, R. P. (1989) *J. Biol. Chem. 264*, 20968−20973.

BI020698O